

Automated systematic evaluation of cryo-EM specimens with SmartScope

Jonathan Bouvette^{1#}, Qinwen Huang^{2#}, Amanda A. Riccio¹, William C. Copeland¹, Alberto Bartesaghi^{2,3,4*} and Mario J. Borgnia^{1*}

¹ Genome Integrity and Structural Biology Laboratory, National Institute of Environmental Health Sciences, National Institutes of Health, Department of Health and Human Services, Research Triangle Park, NC, 27709, USA

² Department of Computer Science, Duke University, Durham, NC, 27708, USA

³ Department of Biochemistry, Duke University School of Medicine, Durham, NC, 27708, USA

⁴ Department of Electrical and Computer Engineering, Duke University, Durham, NC, 27708, USA

These authors contributed equally

* Co-corresponding authors: Mario J. Borgnia and Alberto Bartesaghi

Email: mario.borgnia2@nih.gov, alberto.bartesaghi@duke.edu

Author Contributions: J.B. and M.J.B. developed and implemented SmartScope, Q.H. and A.B. developed and implemented the AI detection and classification for SmartScope. A.A.R. and W.C.C. developed the POLG2 project, including the cloning and purification of the protein. A.A.R. prepared specimens, J.B. and A.R. screened the specimens and collected data. A.A.R. did the data analysis. J.B., Q.H., M.J.B and A.B. wrote the paper, J.B., Q.H. and A.A.R. prepared the figures, and J.B., M.J.B. and A.B. conceived the project.

Keywords: cryo-EM, structural biology, machine-learning, deep-learning, object recognition, software platform.

Abstract

Propelled by improvements in hardware for data collection and processing, single particle cryo-electron microscopy has rapidly gained relevance in structural biology. Yet, finding the conditions to stabilize a macromolecular target for imaging remains the most critical barrier to determining its structure. Attaining the optimal specimen requires the evaluation of multiple grids in a microscope as conditions are varied. While automation has significantly increased the speed of data collection, optimization is still carried out manually. This laborious process which is highly dependent on subjective assessments, inefficient and prone to error, often determines the success of a project. Here, we present SmartScope, the first framework to streamline, standardize, and automate specimen evaluation in cryo-electron microscopy. SmartScope employs deep-learning-based object detection to identify and classify features suitable for imaging, allowing it to perform thorough specimen screening in a fully automated manner. A web interface provides remote control over the automated operation of the microscope in real time and access to images and annotation tools. Manual annotations can be used to re-train the feature recognition models, leading to improvements in performance. Our automated tool for systematic evaluation of specimens streamlines structure determination and lowers the barrier of adoption for cryo-electron microscopy.

Introduction

Over the past decade, advances in hardware and software have established single particle analysis (SPA) cryo-electron microscopy (cryo-EM) as a method of choice in structural biology. The introduction of direct electron detectors combined with advances in computational methods led to improvements in speed and automation of data collection and processing that unleashed an exponential growth in the number of cryo-EM structures deposited in the protein databank. However, preparation of specimens suitable for high-resolution cryo-EM imaging still remains a significant barrier. Consequently, the beginning of each new project is fraught with uncertainty about its duration and probability of success. The ideal specimen for solving a structure by SPA is a single layer of randomly oriented macromolecular complexes embedded into a thin slab of vitreous ice. Current methods for specimen preparation consist in depositing a thin layer of solubilized sample over a special electron microscopy grid and plunging it into liquid ethane cooled to about 83 K. During this process, macromolecules are confined between hydrophobic interfaces with air and other materials composing the substrate. The interaction with the air-water interface can lead to protein denaturation or trap the molecules in a “preferred orientation”, preventing successful structure determination. In addition, these vitrification methods typically yield variations in ice thickness across the grid. These artifacts can severely limit the quality of specimens and are typically addressed through an optimization process in which several parameters are varied to increase the stability and mono-dispersity of the target macromolecule and the uniformity of the ice layer. These include changes to buffer composition during purification and vitrification, and choice of support material and freezing conditions (e.g., temperature, humidity, and blotting paper) (Passmore and Russo, 2016). Testing all combinations at once is impractical because their number grows exponentially with the

inclusion of each parameter. Moreover, the reproducibility of specimen preparation is low and evaluating each combination involves comprehensive sampling of one or more grids using a cryo-electron microscope. Instead, an iterative search is performed in which a limited number of parameters are changed, and the resulting observations are used to determine the ones to be varied in the next cycle.

Specimen screening involves selecting areas for evaluation, adjusting the positioning and optical conditions of the microscope, and recording images at multiple magnifications. The lowest magnifications are used to assess the overall quality of the vitrification process, the number of potential areas amenable to high-resolution data collection and some macroscopic indicators of sample instability such as aggregation. Higher magnification images provide direct information about the macromolecules of interest, such as particle integrity, distribution, density, heterogeneity and orientation, as well as the quality of the ice and the resolution limit of the images. This time-consuming screening process provides valuable information for subsequent iterations of optimization, and the success of a project often depends on the appropriate sampling and interpretation of these results. When performed manually, the implicit subjectivity in the selection of areas can lead to suboptimal sampling, which in turn results in missing information. The time required to manually evaluate each grid varies depending on several factors, but it is estimated to be between 30-60 minutes. The quality of the results, the speed of this labor-intensive process and the integrity of the instrument, all depend on the experience and skills of the operator. Thus, development of a system capable of carrying out these functions automatically in a systematic and unbiased way would be an invaluable tool.

The goal in screening is to gather information from diverse areas of the grid to better understand the behavior of the macromolecules of interest. This contrasts with data collection where the objective is to record areas corresponding to a set of conditions already known to yield the best molecular images. Existing software for automated cryo-EM is optimized for acquiring a large number of images of a pre-selected set of homogeneous targets. Calibrated to allow precise alignment of the different imaging modes for efficient navigation at multiple magnifications, these software packages aim to automatically collect the highest quality images and to maximize throughput, whether for SPA or tomography (Mastrorade, 2005; Suloway et al., 2005). Although semi-automated functions facilitate the detection of holes within a range of intensities, selection and queueing is still performed manually. Following this labor-intensive setup, often comprising the first few hours of a microscopy session, selected areas are automatically collected with minimal supervision for periods usually longer than 12 hours. Screening using these programs, however, would involve a lengthy setup phase for each specimen only to acquire a few targets with marginal gains in speed.

Analysis of screening data consists in evaluating not only high magnification images of the target but also their context. Although all data collection packages preserve lower magnification images and the associated stage positions, they are not designed to facilitate virtual navigation of the grid. Exploring the results in an organized way using programs like EPU, Latitude and SerialEM requires direct access to the local microscope computer, thus limiting their use to times when the instrument is available. A workaround solution is to access the data from a different computer running a dummy instance of the

microscope control software, although this may be limited by licensing of commercial software. Leginon's companion software, Appion (Lander et al., 2009), is a powerful suite for image processing that provides offline access to the results via a web user interface (WebUI). However, none of these packages is optimized for screening nor they provide a web-based solution for controlling the microscope during specimen evaluation. Software and workflows that focus on specimen screening are still needed to streamline bookkeeping and ease the evaluation process.

Here, we present SmartScope, a web-based, highly available expert system capable of doing unsupervised screening of specimens and automated data collection for cryo-EM. SmartScope uses pretrained generalized deep learning models for feature detection and selection to maximize sampling and provide maximal information to guide specimen optimization. By combining automation, machine learning and remote control, we aim to increase the efficiency of the process, reducing costs and dramatically increasing availability. Finally, SmartScope is designed as a modular framework, facilitating the addition of new algorithms for area selection and navigation that can further improve targeting performance.

Main

The complexity of a screening workflow depends on several factors including the instrument used and the type of specimen. Here, we describe the extended operation of a microscope furnished with an autoloader device and loaded with frozen hydrated targets for SPA, which are prepared on a micropatterned holey substrate or continuous carbon (Fig. 1 and S1). All the interactions with the software are carried out using the SmartScope WebUI which also allows to monitor progress and control the workflow with little to no training in cryo-EM. Further, SmartScope permits simultaneous access from multiple remote devices, greatly facilitating collaborative work.

Initialization

After a cassette is inserted in the autoloader, a session is initialized by providing the list of grids to be evaluated along with a series of parameters applicable to all of them (Table S1). SmartScope then initiates a connection to SerialEM (Mastrorade, 2005) via its python API to issue commands to the microscope. This connection is locked to prevent the simultaneous execution of multiple workflows. In instruments equipped with automated loading systems, grids are loaded sequentially into the column and subjected to the operations described in the sections below.

Grid analysis

For each grid loaded, a series of low magnification images are acquired and stitched together to generate a grid map or "Atlas" which is analyzed by SmartScope's deep learning (DL) driven window detector and classifier (Fig 1A). Windows deemed suboptimal for imaging due to physical damage or heavy contamination are excluded from further analysis. The remaining "good" windows are reclassified and clustered based on a selectable criterion (e.g., areas suitable for imaging). Representatives of each window cluster are added to a list of regions of interest (ROIs) with the goal of

adequately sampling the diversity of imageable areas (Fig. 1B). The program then proceeds to visit and select imaging targets from the ROIs in this list, which can be modified via the WebUI at any time before the grid is completed.

Selection of targets

The stage is moved to the next ROI in the list which is brought to eucentric height and imaged at a magnification that ensures complete coverage of the area (Fig. 1A). The next step is to identify targets of interest (TOIs) based on a programmable criterion that depends on the specimen. For example, SmartScope's DL based hole finder is used to detect holes in frozen hydrated SPA specimens. The current algorithm classifies the holes based on their average signal intensity (a proxy for ice thickness) and clusters them into a selectable number of groups. By default, the group containing the darkest targets is rejected as not suitable for imaging. To maximize diversity, holes are selected from the different clusters and added to a TOI list (Fig. 1C). As with ROIs, this selection can be modified at any time during imaging of the grid. A protocol for selecting negative stain TOIs is also available and plug-ins for other types of specimens may be incorporated in the future.

Selected TOIs are visited sequentially by moving the stage to their predicted coordinates. A series of images, at a magnification that encompasses the TOI and surrounding area, are used to recenter the imaging area on the target (a hole in the substrate for SPA). These intermediate resolution images are stored in the database as they often provide valuable information about the specimen, such as affinity of the macromolecules to the support material, aggregation, denaturation, etc. Autofocus and drift stabilization procedures are then performed before acquiring high-magnification images of the target. These newly acquired images are processed using the routine alignframes in IMOD (Kremer et al., 1996) and the program CTFFIND4 (Rohou and Grigorieff, 2015) to facilitate assessment of data quality. This cycle is repeated until all TOIs have been imaged, and the workflow then proceeds to the next ROI.

After all selected ROIs for the grid are finished, SmartScope automatically switches to the next grid. This behavior may be modified by selecting the "pause between grids" option on the session menu. Pausing allows the selection of additional ROIs at the end of the cycle, providing better control of unattended sessions or when evaluating unusual specimens where automated sampling may not be satisfactory.

Accessing and annotating results

SmartScope systematically documents the results and facilitates their analysis. During collection, all images and their related metadata are stored in a consistent data structure. To display and interact with these data, SmartScope implements an intuitive WebUI that tracks the imaging process in real-time. Moreover, it enables remote interaction with a running session, such as modifying area selection, changing labels and acquisition parameters, and taking notes about the specimen, all without interrupting the acquisition workflow.

After a session is over, SmartScope can automatically copy the data to long-term or object storage. The data remains available through the WebUI and allows users to make additional annotations. Other tools, such as micrograph curation and exporting of metadata as star files are also available.

Tools for exhaustive screening and high-throughput data collection

SmartScope can also perform high-throughput data collection. A session can be initialized in data collection mode or changed from screening to data collection by setting the number of TOI to sample to zero. This will have the effect of selecting all the available TOIs for imaging.

To achieve high-throughput, SmartScope makes use of beam-image shift (BIS) for multi-hole imaging (Cheng et al., 2018). BIS can be used during screening for more exhaustive sampling, allowing for exploratory data collections that can provide enough images to carry out 2D classification or initial 3D reconstruction. The BIS grouping in SmartScope uses an algorithm that groups the holes within a given radius (Fig. S2). Only the targets that are labeled as “good” and are in the included clusters are used for the grouping. The algorithm attempts to maximize the coverage of targets while minimizing the total number of groups. To maximize the speed of data collection, a minimal group size can also be specified to prevent the algorithm from assigning small groups of holes.

One way to alleviate the commonly occurring problem of orientation bias in single-particle cryo-EM is to collect data on a tilted specimen (Tan et al., 2017). SmartScope can perform BIS data collection on tilted specimens, where the position and defocus of the targets are corrected using geometrical tilt constraints. This allows for data collection throughput that is similar to regular non-tilted data collection. Moreover, the tilt angle can be seamlessly changed at any point during the acquisition process. Combined with the integrated in-line data processing, this allows to adapt the data collection strategy on-the-fly based on the newly acquired knowledge.

The combination of automated operations such as feature detection routines, multi-hole imaging and tilted data collection capabilities, make SmartScope a powerful tool that can accelerate screening of cryo-EM samples and achieve high-throughput data collection.

Asynchronous imaging and processing

SmartScope was designed to maximize microscope efficiency and to remove much of the idling time in the imaging process. A common source of idling is the processing time required for rendering the frame averages or calculating the CTF fits. To minimize the impact of this, the microscope’s imaging process and the image processing routines run as parallel processes. The newly acquired images or movies are queued up for analysis and processed sequentially on a separate thread. For the atlas and windows, processing includes detecting, classifying, and selecting targets. For high-magnification TOIs, it involves frame alignment and CTF estimation. This allows the microscope to immediately acquire the next target while the images are being analyzed (Fig. S1).

Installation and configuration

SmartScope bundles a webserver and the main imaging workflow. It also relies on a database server to store and query essential metadata (Fig S3). To simplify the deployment and orchestration of these services, we created a Singularity container image that allows rapid deployment on any Linux system.

The application can be installed on a single workstation that will handle the execution of all the services. It can also be installed in a master-worker configuration where, for example, one computer handles the webserver and the database (master), while the main workflow is executed on a workstation that is connected to the microscope network (worker). The minimal requirements are that all the systems can access the database and have access to the main data storage device.

A long-term storage area that holds the data from previous sessions can be specified. Both mounted network drives and object-stores can be used to store the data. This allows to clear data from the main local drives leaving space for the ongoing sessions while keeping older data accessible through the WebUI.

After installation, administrators can login to the WebUI management portal where microscope and detector information needs to be added to allow connection to the instruments. Multiple microscopes can be installed on a single instance of SmartScope, serving as a central hub for microscope access. To access the server, each user has an account and groups are created by an administrator. Users can only access the data from the groups they belong to.

In SerialEM, a settings file containing the magnification for low-dose imaging needs to be prepared for each microscope and detector. The conditions should be set as follows: Full Square image bound to the Search preset; The fine hole re-alignment condition in low SA magnification bound to the View preset; the data acquisition conditions bound to the Record preset with the acquisition and dose fractionation settings bound to the Preview.

Automated object detection and classification

SmartScope identifies and classifies ROIs and TOIs suitable for cryo-EM imaging using DL approaches. At the atlas level, areas suitable for imaging appear as “windows”, commonly shaped as squares, through the metallic grid in which the support layer is intact and not blocked by thick ice or large contaminants. Windows are automatically detected and classified using a pretrained Region-based Convolutional Neural Network (Girshick, 2015) that identifies the “good” windows with 80% precision (Fig. 2A and S4A, Table S2), thus providing information that can effectively guide the instrument to avoid undesirable regions of the grid.

Selected windows are then acquired at a higher magnification where TOIs can take various shapes depending on whether the modality is single particle cryo-EM, tomography or negative stain. In single particle cryo-EM, these TOIs usually show as holes in the substrate and are difficult to detect with traditional image processing tools due to the low contrast, especially when carbon mesh grids are used. We implemented a robust hole detector for frozen specimens based on the You-Only-Look-Once (Redmon et al., 2016) object detection architecture (Fig. 2B and S4B). To prevent the network from incorrectly picking dark ice contaminants, we also added a classification step to separate holes from contaminants and were able to correctly identify 89% of the holes.

Screening mode statistics

In screening mode, the average time required for exchanging specimens and acquiring a partial atlas covering at least 25% of the grid surface is 7.8 min (Fig. 3, Table S4 and S4). The median sampling time for a specimen is 21 min, yielding a median of 9.0 high-

magnification images of holes sampled from 3.0 different windows. Each day, our screening microscope thoroughly screens an average 16 specimens and performs data collection for approximately 16 hours.

Data collection mode statistics

SmartScope offers a convenient option to set up, track data collection and to label and annotate exposures. In data collection mode, the microscope continuously acquires areas and finds targets using operator assistance only to fine tune the selection to specific needs, significantly reducing setup time as compared to our manual workflow. The median data collection setup time, from specimen loading to the start of high-magnification acquisition, is 32 min with our K2 detector (Table S5). As an example, we used SmartScope to determine a 3.4 Å map of the 110 kDa accessory subunit of the human mitochondrial DNA polymerase (Young and Copeland, 2013) (EMD-25764, Fig. 4 and S5). For this specimen, we collected 4,327 micrographs and seamlessly tilted to 30° for the last third of the dataset to improve the angular sampling of the protein.

Discussion

SmartScope is the first package specifically designed to assist, document and automate specimen evaluation during the process of optimizing samples for cryo-EM. The program delivers a unique user experience through a WebUI that provides live remote supervision and control of the screening process using a standard web browser. The same WebUI facilitates analysis of results at any time during and after a session. Multiple users can access the same live or stored session simultaneously and multiple instruments can be controlled from the same server. Automated navigation routines provide control of the microscope without granting full access to functions that may compromise the integrity of the instrument. SmartScope uses fast and robust AI-driven feature recognition algorithms to fully automate the cryo-EM imaging workflow. The steps of target identification, object classification and clustering offer a powerful way to sample a wide variety of areas during screening and help determine the next steps in specimen optimization. This enables complete unsupervised execution of a screening workflow as well as supervised exploration with minimal user training.

SmartScope can also collect data in a semi-supervised or fully automated way. The areas automatically selected by SmartScope can be modified interactively or programmatically without interrupting the process of data collection. This maximizes the use of the microscope and offers the possibility of integrating feedback from in-line data processing workflows to adaptively improve image quality during acquisition, without user intervention. Unsupervised multi-specimen screening and short exploratory data collection sessions can be scheduled to run overnight, offering new ways of using the microscope.

SmartScope has a modular design where new object detection and classification algorithms can be added as plugins, allowing integration of existing object detection and area selection programs for cryo-EM (Fan et al., 2022; Kim et al., 2021; Rheinberger et al., 2021; Xu et al., 2020; Yokoyama et al., 2020; Yonekura et al., 2021). Additionally, the ability to use multiple feature detection and clustering methods at different

magnification levels enables the creation of customized protocols for specific applications. This provides flexibility to optimize selection of areas on a wider variety of targets in cryo-EM, such as virions, filaments and cells. Finally, as we gather more data about difficult specimens and edge cases, we envision the establishment of a globally accessible “virtual microscopist” server capable of improving itself through periodic re-training based on voluntarily submitted labeled datasets.

SmartScope has proven to be an extremely valuable tool in our facility. It has streamlined bookkeeping, which in turn resulted in better decision making for specimen optimization. It has also maximized microscope usage by eliminating idling time, reducing setup and screening times. SmartScope facilitates data and instrumentation access as well as collaboration by easing access to cryo-EM technologies and improving the way cryo-EM experiments are carried out. With specimen screening as a primary focus, SmartScope addresses an important limiting step in cryo-EM.

Materials and methods

Cryo-Electron Microscopy

All the data presented in this study was acquired on a Talos Arctica (Thermo Fisher Scientific) operating at 200 kV and equipped with a K2 direct-electron detector (Gatan Inc.). SmartScope was also tested on a Ceta CMOS detector and a Titan Krios (Thermo Fisher Scientific) equipped with a K3 detector and BioQuantum energy filter (Gatan Inc.). The statistics were derived from data acquired exclusively with the K2 detector. For microscope and detector control, SmartScope uses SerialEM 4.0 through the python API library (Mastronarde, 2005).

Square Finder

To localize and classify square windows, a faster R-CNN-based framework (Girshick, 2015) that uses a ResNet50 architecture as the feature extraction backbone was adopted. It incorporates a feature pyramid network for identification of objects at different magnification levels. In addition, since most features have approximately equal width and height, the bounding boxes were constrained to have aspect ratios within the 0.8 to 1.2 range. To improve robustness and stability of the model, data augmentation was applied to the training data, including zoom-in/zoom-out, rotation, contrast adjustments and flipping. The degree of augmentation for the contrast intensity was limited to the 0.8 and 1.2 range. To compensate for label imbalance, random oversampling was added during training. Squares are classified into 6 different classes: good (suitable for imaging), small (thick ice), contaminated, cracked, fractioned, and broken. The low-level magnification feature detector was trained using a total of 12 atlases from both carbon and gold mesh grids. Each atlas contains around 50 to 100 squares on average. The original atlases, usually having widths and heights greater than 10,000 pixels were downsampled to 2048 x 2048 pixels to reduce memory requirements. The framework is implemented using the python library Detectron2 (Wu et al., 2019). Training the detector takes around 2 hours when running on a NVIDIA TITAN V GPU card with 32GB of RAM. The pre-trained weights are then used for fast real-time square detection during screening, which can evaluate each atlas image in under a second.

Hole Finder

To identify holes on all grid types and contrast levels, a deep neural-network architecture based on the YOLOv5 model was adopted (Jocher et al., 2020; Redmon et al., 2016). We used the Cross Stage Partial Network (CSPNet) (Wang et al., 2019) as the feature extraction backbone and standard convolutional layers as detection layers. Since holes have circular shapes, the aspect ratios of the bounding boxes were also constrained. To further facilitate training, instead of using arbitrary numbers for anchor bounding boxes generation, clustering algorithms to the ground truth boxes from the training dataset were applied to find the most common occurring sizes and we used these sizes to determine the anchor bounding box sizes. Data augmentation was applied during training, including: contrast/brightness adjustment, rotation/translation, zoom-in/zoom-out, and cropping. To deal with small contamination areas that can be incorrectly detected as holes, an additional “contaminants” class is used to filter out such areas. Training of the hole finder was done using 32 square images and took 1.5 hours when running on a NVIDIA TITAN V GPU card with 32GB of RAM and inference takes less than a second. For memory efficiency, each square was resized to 1280x1280 pixels.

POLG2 purification

Protein was expressed and purified essentially as described (Young et al., 2015) with the following exception: Triton-X was removed from all steps following lysis. Following Ni purification, pooled protein containing His₆-POLG2, as determined by SDS-PAGE, was injected onto a monoS column. Protein was eluted from S column in a linear gradient from 5% to 50% Buffer B (25 mM HEPES, 1 M NaCl, 10% glycerol, 1 mM EDTA, 1 mM TCEP). Peak fractions were eluted around 310 mM NaCl. Fractions were checked for purity, combined and concentrated using an Amicon concentrator (Millipore) to 28 μ M. Protein is flash frozen and stored at -80 °C.

4.1 μ M (monomer) his-tag POLG2 was incubated in a 1:1 molar ratio with FORK1 DNA as previously described (6) Oligonucleotides: (i) DCRANDOM- 44
ACTTGAATGCGGCTTAGTATGCATTGTAAAACGACGGCCAGTGC (2) TSTEM
GCACTGGCCGTCGTTTTACGGTCGTGACTGGGAAAACCCTGGCG (3) U25
CGCCAGGGTTTTCCCAGTCACGACC were all purchased from IDT. Protein in a final buffer of 20 mM HEPES pH 8, 1.5 mM Tris pH 7.5, 30 mM KCl, 50 mM imidazole pH 8, 0.3 mM EDTA, 225 mM NaCl, 1.5% glycerol, 1 mM TCEP was incubated on ice for approximately 30 minutes before grid application.

Cryo-EM specimen preparation

UltraAUfoil R1.2/3 (Quantifoil Micro Tools GmbH) grids were glow-discharged on both sides for 30 s at 15 mA using a Pelco Easiglow. 3 μ L of the final buffer was deposited on the back of the grid and 3 μ L of POLG2 sample was deposited on front side of the grid. Excess sample was blotted 4 s with blotting force -1, the chamber set at 12 °C and 95% humidity using a Vitrobot Mark IV (Thermo Fisher Scientific).

Data collection of POLG2 with SmartScope

Data was collected on a Talos Arctica (Thermo Fisher Scientific) operating at 200 kV equipped with a Gatan K2 direct electron detector (Gatan Inc.). Data collection was set up using SmartScope using a 6x6 tile atlas, image-shift grouping radius of 4 μ m and

minimum group size of 4 holes, rolling target defocus of -1.2 to -1.8 μm and drift settling threshold at 1 $\text{\AA}/\text{s}$. A total of 4,311 60-frame movies were collected at a 0.932 $\text{\AA}^2/\text{pixel}$ and total dose of 54 $\text{e}^-/\text{\AA}^2$. 3,029 movies were collected at 0° tilt angle and 1,282 movies were collected with 30° tilt angle. Data was collected at a rate of 120 movies per hour.

Cryo-EM data processing and refinement

The POLG2 dataset was processed using cryoSPARC (Punjani et al., 2017) as detailed in Fig. S5C. Final maps were sharpened using DeepEMhancer (Sanchez-Garcia et al., 2021). An atomic model from PDB ID: 2G4C (Fan et al., 2006) was fit into the map using Chimera (Pettersen et al., 2004).

Code availability

SmartScope is undergoing a closed beta program. For information about enrollment, please visit <https://docs.smartscope.org/>.

Acknowledgments

This work was supported in part by the Intramural Research Program of the NIH; National Institute of Environmental Health Sciences (ZIC ES103326 and ZIA ES103341 to M.J.B., and Z01 ES065078 to W.C.C.). This work utilized cloud computational resources and services accessed through the NIH STRIDES Initiative (<https://cloud.nih.gov>) and computational resources offered by Duke Research Computing (<http://rc.duke.edu>). We thank Tracy Futhey, Charley Kneifel, Katie Kilroy, Mike Newton, Victor Orlikowski, Tom Milledge, and David Lane from the Duke Office of Information Technology and Research Computing for assistance with the computing environment. We also thank David Fargo, John Grovenstein and Chris Stone from the NIEHS Office of Scientific Computing for allocating computational resources to this project and especially to Gregory Stamper for assistance in setting up computing environments. We also thank Dr. Joshua Strauss from the UNC cryo-EM Core and Dr. Nilakshee Bhattacharya from the Duke Shared Material Instrumentation Facility (SMIF) for testing early versions of SmartScope. Molecular graphics and analyses performed with UCSF Chimera, developed by the Resource for Biocomputing, Visualization, and Informatics at the University of California, San Francisco, with support from NIH P41-GM103311. We thank Robin E. Stanley and Bradley P. Klemm for critical review of the manuscript.

Competing interests

The authors declare no competing interests.

References

- Cheng, A., Eng, E.T., Alink, L., Rice, W.J., Jordan, K.D., Kim, L.Y., Potter, C.S., Carragher, B., 2018. High Resolution Single Particle Cryo-Electron Microscopy using Beam-Image Shift. *J. Struct. Biol.* 204, 270–275. <https://doi.org/10.1016/j.jsb.2018.07.015>
- Fan, L., Kim, S., Farr, C.L., Schaefer, K.T., Randolph, K.M., Tainer, J.A., Kaguni, L.S., 2006. A Novel Processive Mechanism for DNA Synthesis Revealed by Structure, Modeling and Mutagenesis of the Accessory Subunit of Human Mitochondrial DNA Polymerase. *J. Mol. Biol.* 358, 1229–1243. <https://doi.org/10.1016/j.jmb.2006.02.073>
- Fan, Q., Li, Y., Yao, Y., Cohn, J., Liu, S., Vos, S.M., Cianfrocco, M.A., 2022. CryoRL: Reinforcement Learning Enables Efficient Cryo-EM Data Collection. *ArXiv220407543 Cs Q-Bio*.
- Girshick, R., 2015. Fast R-CNN. *ArXiv150408083 Cs*.
- Jocher, G.R., Stoken, A., Borovec, J., NanoCode, ChristopherSTAN, Changyu, L., Laughing, Hogan, A., lorenzomamma, tkianai, yxNONG, AlexWang, Diaconu, L., Marc, wanghaoyang, ah, ml, Doug, Hatovix, Poznanski, J., 于力军 L.Y., Changyu, Rai, P., Ferriday, R., Sullivan, T., Xinyu, W., YuriRibeiro, Claramunt, E.R., hopesala, Dave, P., yzchen, 2020. *ultralytics/yolov5: v3.0*.
- Kim, P.T., Noble, A.J., Cheng, A., Bepler, T., 2021. Learning to automate cryo-electron microscopy data collection with Ptolemy. *ArXiv211201534 Cs Eess Q-Bio*.
- Kremer, J.R., Mastronarde, D.N., McIntosh, J.R., 1996. Computer Visualization of Three-Dimensional Image Data Using IMOD. *J. Struct. Biol.* 116, 71–76. <https://doi.org/10.1006/jsbi.1996.0013>
- Lander, G.C., Stagg, S.M., Voss, N.R., Cheng, A., Fellmann, D., Pulokas, J., Yoshioka, C., Irving, C., Mulder, A., Lau, P.-W., Lyumkis, D., Potter, C.S., Carragher, B., 2009. Appion: an integrated, database-driven pipeline to facilitate EM image processing. *J. Struct. Biol.* 166, 95–102. <https://doi.org/10.1016/j.jsb.2009.01.002>
- Mastronarde, D.N., 2005. Automated electron microscope tomography using robust prediction of specimen movements. *J. Struct. Biol.* 152, 36–51. <https://doi.org/10.1016/j.jsb.2005.07.007>
- Passmore, L.A., Russo, C.J., 2016. Chapter Three - Specimen Preparation for High-Resolution Cryo-EM, in: Crowther, R.A. (Ed.), *Methods in Enzymology, The Resolution Revolution: Recent Advances In CryoEM*. Academic Press, pp. 51–86. <https://doi.org/10.1016/bs.mie.2016.04.011>
- Pettersen, E.F., Goddard, T.D., Huang, C.C., Couch, G.S., Greenblatt, D.M., Meng, E.C., Ferrin, T.E., 2004. UCSF Chimera—A visualization system for exploratory research and analysis. *J. Comput. Chem.* 25, 1605–1612. <https://doi.org/10.1002/jcc.20084>
- Punjani, A., Rubinstein, J.L., Fleet, D.J., Brubaker, M.A., 2017. cryoSPARC: algorithms for rapid unsupervised cryo-EM structure determination. *Nat. Methods* 14, 290–296. <https://doi.org/10.1038/nmeth.4169>
- Redmon, J., Divvala, S., Girshick, R., Farhadi, A., 2016. You Only Look Once: Unified, Real-Time Object Detection. *ArXiv150602640 Cs*.

- Rheinberger, J., Oostergetel, G., Resch, G.P., Paulino, C., 2021. Optimized cryo-EM data-acquisition workflow by sample-thickness determination. *Acta Crystallogr. Sect. Struct. Biol.* 77, 565–571. <https://doi.org/10.1107/S205979832100334X>
- Rohou, A., Grigorieff, N., 2015. CTFFIND4: Fast and accurate defocus estimation from electron micrographs. *J. Struct. Biol., Recent Advances in Detector Technologies and Applications for Molecular TEM* 192, 216–221. <https://doi.org/10.1016/j.jsb.2015.08.008>
- Sanchez-Garcia, R., Gomez-Blanco, J., Cuervo, A., Carazo, J.M., Sorzano, C.O.S., Vargas, J., 2021. DeepEMhancer: a deep learning solution for cryo-EM volume post-processing. *Commun. Biol.* 4, 1–8. <https://doi.org/10.1038/s42003-021-02399-1>
- Suloway, C., Pulokas, J., Fellmann, D., Cheng, A., Guerra, F., Quispe, J., Stagg, S., Potter, C.S., Carragher, B., 2005. Automated molecular microscopy: The new Leginon system. *J. Struct. Biol.* 151, 41–60. <https://doi.org/10.1016/j.jsb.2005.03.010>
- Tan, Y.Z., Baldwin, P.R., Davis, J.H., Williamson, J.R., Potter, C.S., Carragher, B., Lyumkis, D., 2017. Addressing Preferred Specimen Orientation in Single-Particle Cryo-EM through Tilting. *Nat. Methods* 14, 793–796. <https://doi.org/10.1038/nmeth.4347>
- Wang, C.-Y., Liao, H.-Y.M., Yeh, I.-H., Wu, Y.-H., Chen, P.-Y., Hsieh, J.-W., 2019. CSPNet: A New Backbone that can Enhance Learning Capability of CNN. *ArXiv191111929 Cs*.
- Wu, Y., Kirillov, A., Massa, F., Lo, W.-Y., Girshick, R., 2019. Detectron2.
- Xu, H., Timm, D.E., Elhabian, S.Y., 2020. Attention-Guided Quality Assessment for Automated Cryo-EM Grid Screening, in: Martel, A.L., Abolmaesumi, P., Stoyanov, D., Mateus, D., Zuluaga, M.A., Zhou, S.K., Racocanu, D., Joskowicz, L. (Eds.), *Medical Image Computing and Computer Assisted Intervention – MICCAI 2020, Lecture Notes in Computer Science*. Springer International Publishing, Cham, pp. 56–65. https://doi.org/10.1007/978-3-030-59722-1_6
- Yokoyama, Y., Terada, T., Shimizu, K., Nishikawa, K., Kozai, D., Shimada, A., Mizoguchi, A., Fujiyoshi, Y., Tani, K., 2020. Development of a deep learning-based method to identify “good” regions of a cryo-electron microscopy grid. *Biophys. Rev.* 12, 349–354. <https://doi.org/10.1007/s12551-020-00669-6>
- Yonekura, K., Maki-Yonekura, S., Naitow, H., Hamaguchi, T., Takaba, K., 2021. Machine learning-based real-time object locator/evaluator for cryo-EM data collection. *Commun. Biol.* 4, 1–8. <https://doi.org/10.1038/s42003-021-02577-1>
- Young, M.J., Copeland, W.C., 2013. Mitochondrial Disorders Associated with the Mitochondrial DNA Polymerase γ : A Focus on Intersubunit Interactions, in: Wong, L.-J.C. (Ed.), *Mitochondrial Disorders Caused by Nuclear Genes*. Springer, New York, NY, pp. 49–72. https://doi.org/10.1007/978-1-4614-3722-2_3
- Young, M.J., Humble, M.M., DeBalsi, K.L., Sun, K.Y., Copeland, W.C., 2015. POLG2 disease variants: analyses reveal a dominant negative heterodimer, altered mitochondrial localization and impaired respiratory capacity. *Hum. Mol. Genet.* 24, 5184–5197. <https://doi.org/10.1093/hmg/ddv240>

Figures

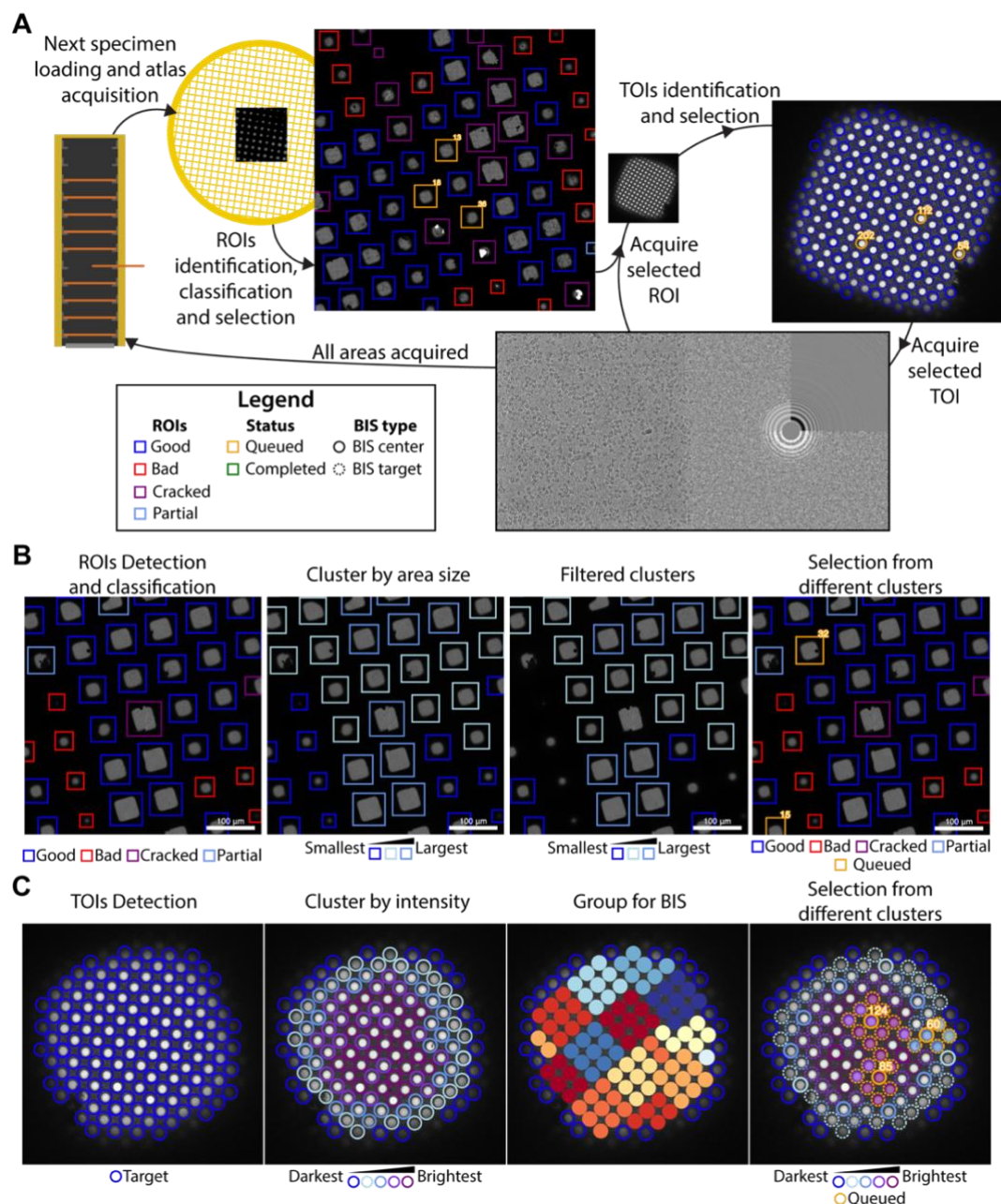


Figure 1. Overview of the SmartScope framework. **A.** Workflow for unsupervised grid navigation and imaging. SmartScope handles specimen exchange, atlas acquisition, ROI identification, classification, and selection. It then visits the selected regions and identifies and selects TOIs which are acquired at higher magnification and preprocessed. **B.** Detailed steps in ROI selection. After detection and classification, ROIs are also clustered into groups. In the example is a clustering by size. Then, from the ROIs are queried based on their class and ROIs from different clusters are selected. **C.** Detailed steps in TOI selection. Shown here is the hole detection followed by a median intensity clustering. Then, holes are grouped by image-shift radius and groups from each cluster are selected for imaging.

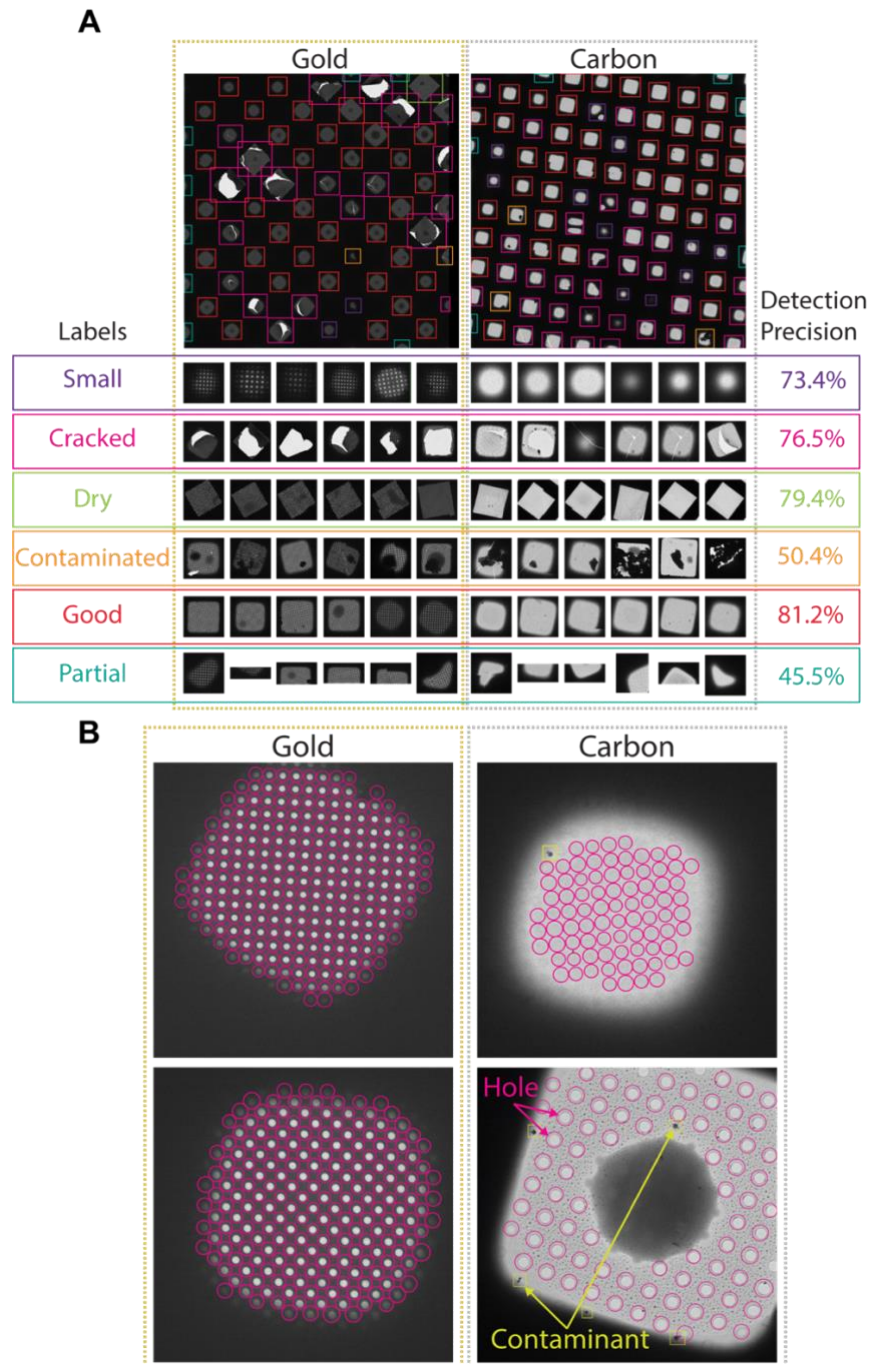


Figure 2. Deep-learning-based feature recognition for autonomous grid navigation. Sample images show the performance of the square (**A**) and hole (**B**) detectors applied to gold (left) and carbon (right) grids. **A.** Automatic detection of squares and classification into six different classes: small, cracked, dry, contaminated, good and partial. Representative examples of squares assigned to each class and corresponding detection precision values are shown (bottom panel). **B.** Hole detection performance on representative square images extracted from gold and carbon grids. The hole detector implements a classification step to filter out contaminants (shown in yellow) and increase hole detection precision (shown as pink circles).

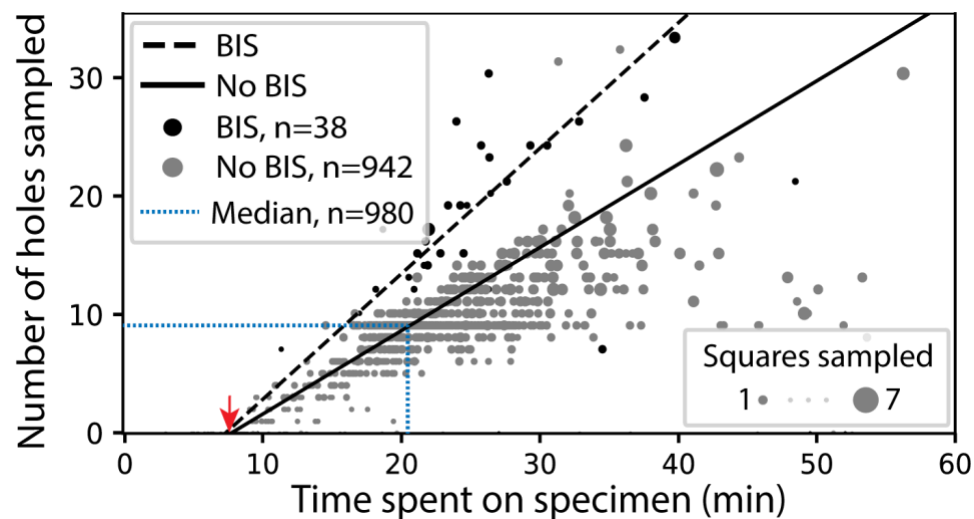


Figure 3. SmartScope's screening mode statistics. Screening rates with and without beam-image shift (BIS) were 1.0 and 0.7 holes per minute respectively (RANSAC regression). The red arrow indicates the time of specimen loading and start of atlas acquisition. Dashed blue line represents the median session duration (21.6 min) and the median number of high-magnification images (9.0) obtained per specimen during screening mode.

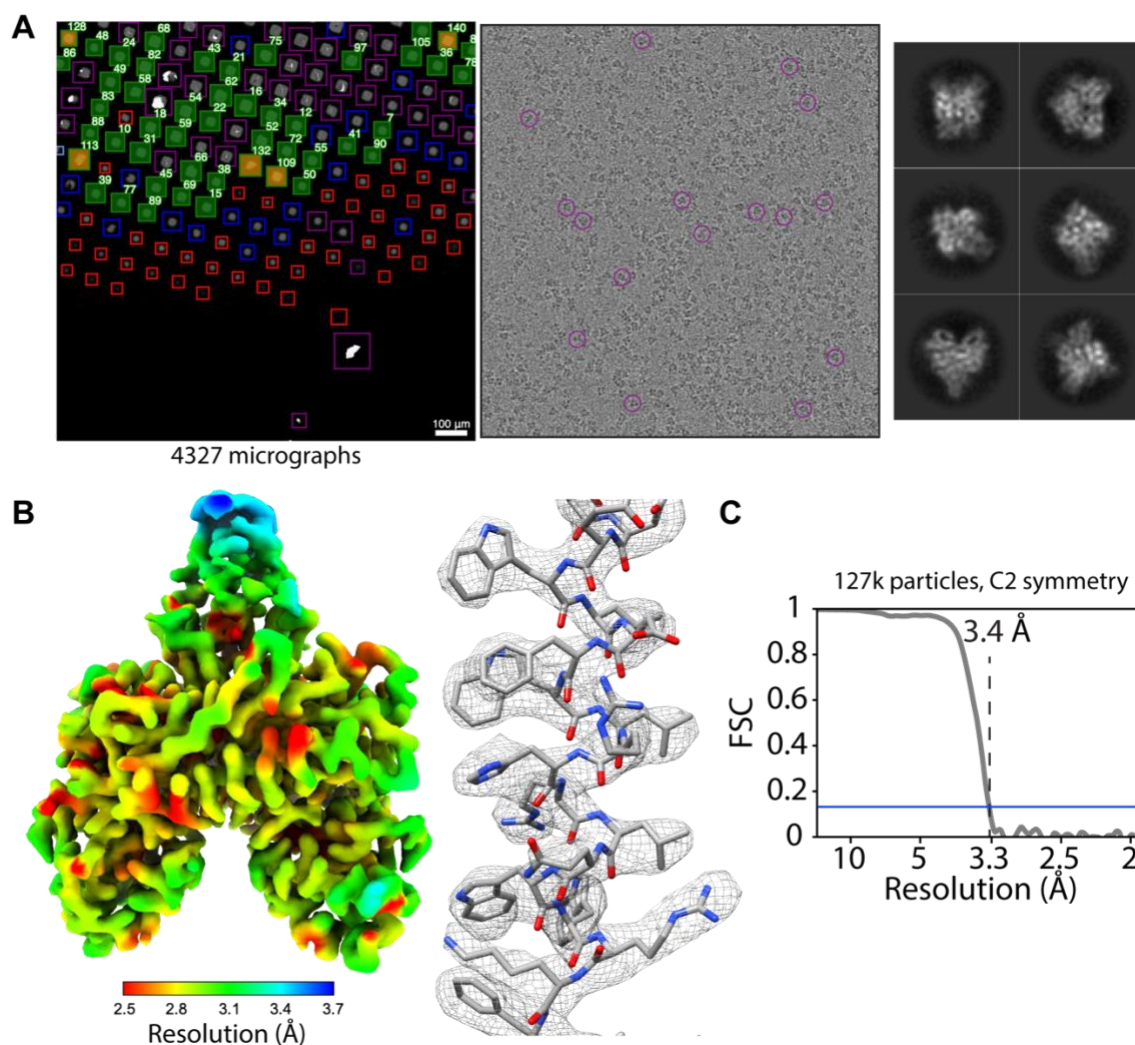


Figure 4. Acquisition of POLG2 dataset using SmartScope. **A.** Atlas of the specimen (left), typical micrograph (center) with some particles picked (purple circles) and 2D classes of POLG2 (right). **B.** Resulting map of POLG2 colored by local resolution (left) and example of an alpha helix with atomic model fit into the density (left). **C.** Fourier-shell correlation curve between half-maps showing a resolution of 3.4 Å.